Oxid Met (2017) 87:617–629
DOI 10.1007/s11085-017-9766-9

ORIGINAL PAPER

Kinetics of Duplex Oxide Growth on 9Cr Steels Exposed in CO_2: Application of Dimensional Metrology

Joy Sumner[1] · Nigel Simms[1] · Aya Shin[2] · Jonathan Pearson[2]

Received: 23 February 2017 / Published online: 5 April 2017

Abstract Investigations into potentially extending the lives of UK advanced gas-cooled reactors have highlighted the need for improved understanding of the long-term oxidation and carburisation of 9Cr ferritic steels. These steels were used in evaporators and primary superheaters and as these are to be used beyond their original design lives, it is necessary to ensure that these degradation routes remain within acceptable levels. A dimensional metrology technique has been applied to archived autoclave samples to measure such damage. These samples had previously been exposed to a range of temperatures, pressures and gas chemistries representative of those experienced by 9Cr steels in CO_2-rich AGR gases. Earlier sample assessments had focused on weight change measurements, but the dimensional technique enables measurement of duplex oxide thicknesses around samples and the extraction of related data from longer exposure times. These data also support estimation of the extent of both carbon and oxygen uptake.

Keywords CO_2 corrosion · 9Cr steel · Duplex oxide · Carburisation

✉ Joy Sumner
j.sumner@cranfield.ac.uk

Nigel Simms
n.j.simms@cranfield.ac.uk

Aya Shin
aya.shin@edf-energy.com

Jonathan Pearson
jonathan.pearson@edf-energy.com

[1] Cranfield University, Cranfield, Bedfordshire MK43 0AL, UK

[2] EDF Energy Generation, Barnwood, UK

Introduction

Currently the potential to extend the operational lives of UK-based AGR (advanced gas-cooled reactor) plants is being considered. The case for such an extension depends upon the remnant life of a number of key components within the reactors, including the evaporators and primary superheaters, which were constructed using 9Cr-1Mo ferritic steels [1–4]. These steels were chosen due to their good resistance to oxidation/carburisation and stress corrosion during their design lifetimes, as well as having reasonable mechanical and welding properties [1–3].

The 9Cr steel heat exchangers in the AGRs were designed for an operational environment with a CO_2-based coolant and metal temperatures of 480-520 °C/gas pressures of 41 bar [1, 4, 5]. The CO_2-based coolant also contained $\sim$1% CO and trace amounts of $H_2/H_2O/CH_4$ (at 100 s vppm levels). It was anticipated that while these conditions would result in oxidation/carburisation of the 9Cr-1Mo steels [1, 6], the ensuing metal loss could be well defined. Furthermore, the coolant gas composition would cause a suitable balance of core graphite corrosion and carbon deposition. Initial AGR designs anticipated lifetimes of 250 khour, resulting in 9Cr-1Mo steel metal losses of the order of 250 μm at 520 °C [1, 3]. However, for plant life extension cases, the impact of oxidation/carburisation on these steels at longer exposure times must be considered.

Following initial transient behaviour, the oxidation/carburisation processes that the 9Cr-1Mo ferritic steels are anticipated to undergo are, for long periods, of a semi-protective nature. The semi-protective oxidation product formed is a duplex scale with an outer magnetite (Fe_3O_4) and inner spinel ($(Fe,Cr)_3O_4$) layer [6–8]. The magnetite grows by the outward diffusion of Fe cations, according to Eq. 1, while the spinel layer forms by the inward diffusion of oxidising species which react at the metal/inner oxide interface [6–8]. Currently the inwardly diffusing oxidant species is not defined, although both carbon and oxygen are transported; thus, the metal/oxide interface reaction can be described by more general Eq. 2. The spinel layer determines the rate of oxidation under duplex growth [6, 9]. Below the duplex layer, an internal oxidation zone (IOZ) can often be observed, and below that the base metal alloy undergoes carburisation [1, 6, 9, 10].

$$3\mathrm{Fe} + 2\mathrm{O}_2 \leftrightarrow \mathrm{Fe}_3\mathrm{O}_4 \tag{1}$$

$$3\ (\mathrm{Fe},\mathrm{Cr},\mathrm{Mo}) + 4\mathrm{O} + x\mathrm{C} \leftrightarrow (\mathrm{Fe},\mathrm{Cr},\mathrm{Mo})_3\mathrm{O}_4 + x\mathrm{C} \tag{2}$$

Mechanistically, many of the atomic-level processes which result in this microstructure are still undergoing investigation. In the duplex layer, the magnetite grows outwards and the spinel inwards (consuming metal cross section), with the original metal surface remaining at the magnetite/spinel interface [13, 33]. Thus, for spinel growth to occur, oxidants must reach the oxide/metal interface [9, 11, 12]. CO_2/CO and H_2O/H_2 are some of the oxidant species which could potentially be responsible for the continued growth of spinel, while if the Boudouard reaction is significant, carbon from CO could be injected into the base metal alloy [7, 9, 11, 13]. It is also known that within the semi-protective growth regime,

iron diffusion across this spinel layer appears to control the oxidation rate [6, 9]. The rate of duplex oxide growth on 9Cr-1Mo steels in AGR conditions, and its stability can depend on many factors, including: minor elements within the alloy such as silicon [9, 13–17], sulphur [18], and phosphorus [14, 18]; metal temperatures [4, 9, 18]; CO in the AGR gas [1, 19]; and H_2O in the AGR gas [18–21].

Current models for the growth of duplex oxides in AGR environments are usually based on rate laws and oxidation activities. However, the underlying data for extracting these parameters often come from weight change measurements [10, 17, 22]. While this allowed rapid, non-destructive evaluation of the oxidation's extent, it also acts to 'average out' any variation in oxidation/carburisation effects across an entire sample and is disrupted by breakaway oxidation. As several studies have noted that oxidation/carburisation does not always progress at a uniform and identical rate around specimens/components [13, 14, 17, 33], this 'averaging' can limit the accuracy of duplex oxide growth model parameters. This is even more important when, due to the parallel carburisation processes that are underway, carbon is also incorporated into the base alloy and contributing significantly to the total weight change.

After the AGR plants were built, a further driver to develop accurate models of duplex oxide growth and associated carbon uptake was discovered. At elevated temperatures (compared to AGR operation), the localised breakdown of duplex oxide growth occurs after long exposures, resulting in more rapid oxidation with near linear growth kinetics [6, 13, 19, 21, 23]. The mechanistic trigger for this 'breakaway oxidation' process is under active investigation, but some proposed mechanisms include a critical carbon uptake level below the duplex oxide scale.

An improved understanding of 9Cr-1Mo ferritic steel's oxidation and carburisation mechanisms will thus give both industry and researchers useful insights. In particular, the quantitative investigation of the variation in oxide scale around different samples is needed to understand the spread in oxide thicknesses, including when some areas of samples are experiencing breakaway. These data could provide the basis for building oxidation kinetics models, and verifying them at longer exposure times than is currently possible using weight change-related data, where large changes from small fractions of the surface undergoing breakaway oxidation currently distort trends.

Experimental Procedures

Sample Supply

EDF Energy has produced an extensive range of autoclave samples since the AGRs were constructed in the 1960s. Many of these tests have been 'accelerated' by the use of higher-than-operational metal temperatures. These test programmes have run for considerable lengths of time, up to 30 khours, with material periodically cut from the main samples for archiving.

The 9Cr-1Mo ferritic steels for the autoclave tests came from batches supplied to AGR plants (Table 1). Examples of these were samples consisting of segments of

Table 1 Steel composition for the 2 sample types in weight %. Balance Fe

Batch	Cr	S	Si	Mn	P	C	Mo	Ni	Co	Cu	Ni	Ti	V	W
Finned	9.2	0.008	0.67	0.47	0.011	0.093	1.04	0.2	0.02	0.16	<0.02	<0.02	<0.05	<0.05
Plain	8.6	0.007	0.42	0.43	0.010	0.083	0.99	0.2	0.02	0.09	<0.02	<0.02	<0.05	<0.05

either plain or finned tube. Finned tubes typically had 3 fins per sample. Within the autoclave test programme, various exposure parameters were investigated (Table 2). The exposure environment was a CO_2 gas with various additions (Tables 3, 4) including a trace 'moisture' content (actually $H_2O + H_2$). It should be noted that the environment undergoes gas conditioning to meet specific targets related to plant operations and so is deliberately not at equilibrium condition; as such, local oxygen partial pressures need to be calculated using redox reactions (for methodology see, for example, [7, 8]). For both moisture contents, this gives oxygen partial pressures in the range of 10^{-21} bar (at 600 °C) to 10^{-19} bar (at 650 °C).

Previous analysis of these samples involved: weight change measurements, visual monitoring and occasional destructive analysis (for cross-sectional investigation). This paper assesses the suitability of an image analysis-based dimensional metrology technique for reassessing these archived samples.

Sample Preparation

To analyse the oxide scale thicknesses, sample cross sections were required. As the samples analysed in this paper were archived samples, many had previously been mounted in Bakelite (using hot isostatic pressing). Where this was not the case, samples were mounted in a low shrinkage resin (50:50 mix of Struers' Epofix low shrinkage resin and ballotini; glass spheres with diameters of ~40–70 μm) and vacuum impregnated before being cross-sectioned. The cross-sectioned samples were prepared or re-prepared using UK #1200 grit to remove any surface degradation/scratches followed by polishing with 6 μm diamond cloth and colloidal silica, resulting in a surface suitable for optical microscopy.

Analysis Technique

Over approximately 35 years, a measurement system based on image analysis of optical micrographs has been developed to investigate metal loss and related coating/deposit/internal damage layer thicknesses. Initial development took place at British Coal/CEGB and Cranfield University via the 'Grimethorpe Topping Cycle Project' and an EU JOULE programme on the erosion/corrosion of materials for power generation systems [24, 25]. Optimisation of this technique has been reported elsewhere [26–29] and has been applied particularly to materials for use in jet

Table 2 Autoclave exposure parameters

Parameter	Autoclave test range	Range for reported samples
Temperature	520–640 °C	600, 620, 640 °C
Gas pressure	600 and 450 psig (41 and 31 bar or 4.1 and 3.1 MPa)	600 psig (41 bar or 4.1 MPa)
Exposure time	240–20, 692 h	240–20, 692 h

Table 3 Non-equilibrium gas composition for 'low moisture' gas

	CO_2	CO	H_2	H_2O	CH_4
Composition	Balance	1%	100 vppm	300 vppm	300 vppm
Partial pressure (kPa)	4060	41	0.41	1.23	1.23

Table 4 Non-equilibrium gas composition for 'medium moisture' gas

	CO_2	CO	H_2	H_2O	CH_4
Composition	Balance	1%	100 vppm	700 vppm	300 vppm
Partial pressure (kPa)	4060	41	0.41	2.87	1.23

engines, industrial gas turbines and pulverised fuel combustion heat exchanger tubing.

Figure 1 shows the traditional use of this technique: (a) a sample is measured pre-exposure; (b) the sample is then tested and sectioned; (c) placed on an x–y calibrated microscope stage (Leitz Wetzlar optical microscope) with a bespoke automated image analyser subroutine to collect evenly spaced images from the sample; (d) key points on the micrographs are selected (e.g. remaining metal, internal damage and coating interfaces.); (e) this allows the pre- & post-exposure sample shapes to be compared; (f) around the samples a range of different metal losses or scale/oxide/internal damage thicknesses will be acquired; (g) ordering the data from most to least damaged produces 'cumulative probability of damage' charts for ease of data manipulation [31, 32]. To improve statistical analysis, data

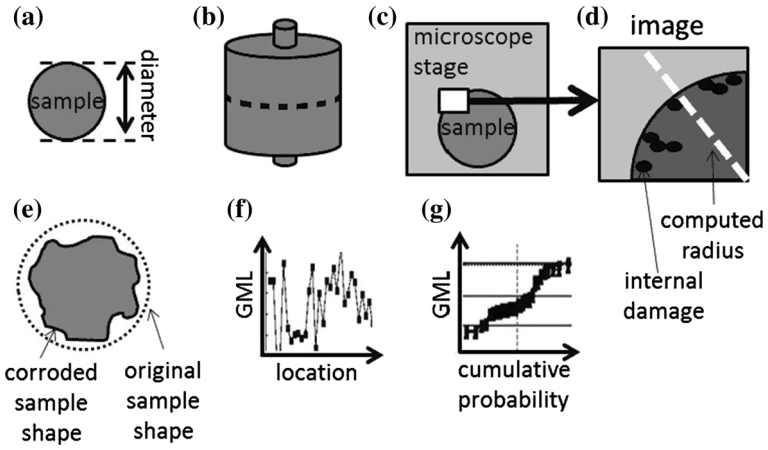

Fig. 1 Dimensional metrology method to determine metal loss [30]

should be taken from >24 locations per region of behaviour. The data are plotted against cumulative normal distribution (in standard deviations; std dev) and give a metal loss error of approximately ±5 μm.

For this work, three major variations on this standard procedure were required, as discussed previously [33]:

- Firstly, as the samples were taken from archives and had already been exposed, pre-exposure dimensional measurements did not exist. However, the spinel/magnetite interface of duplex scales can be taken as the initial, unexposed surface's location in areas where the oxidation has not progressed to breakaway [13, 34]. Where the sample had progressed to breakaway, initially little distortion of the inner/outer oxide interface was observed; the distortion only became significant as breakaway progressed. However, key information such as metal loss (change in fin shape) and changing outer magnetite to inner 'spinel' layer ratios could still be measured in these, more significant breakaway, instances.
- Secondly, the finned samples were analysed by taking each fin separately (to enable automated data collection of a complex shape). As such, ~48 datasets were collected for each fin or planar sample.
- Finally, mosaics of 9 micrographs were collected, and then on each of these, four lines were plotted perpendicular to the original metal surface. On each line, 4 points were recorded (equivalent to Fig. 1d): the outer magnetite surface; the magnetite/spinel interface; the spinel/metal interface; and any observable IOZ.

Results and Discussion

This paper uses a subset of the collected data to illustrate the overall analysis process and the variation in duplex oxide growth (Initial Measurements Section). Following on from this, the effects of different parameters on duplex oxide growth are considered using subsets of the dataset (Effect of Exposure Condition Section). Finally, trends identified using the entire dataset are used as the basis for a discussion on carbon injection (Discussion Relating to Carbon Injection).

Initial Measurements

Figure 2a, b shows examples of oxide thickness variations around different samples exposed in autoclaves at elevated temperatures for accelerated testing (600 °C c.f. AGR operation at ~520 °C). In particular, significant variation can be observed within fins in terms of duplex and breakaway oxidation. The breakaway oxidation characteristically nucleates at the fin tip, propagating down along the fin length with extended exposure time. Figure 2c, d shows the spinel/metal interface, giving an indication of how metal is consumed over time. It should be noted that different fins are consumed at different rates and that the tube wall itself shows no signs of the rapid metal consumption linked to breakaway oxidation. This variation continues with increased exposure time, here from 12,877 to 19,924 h.

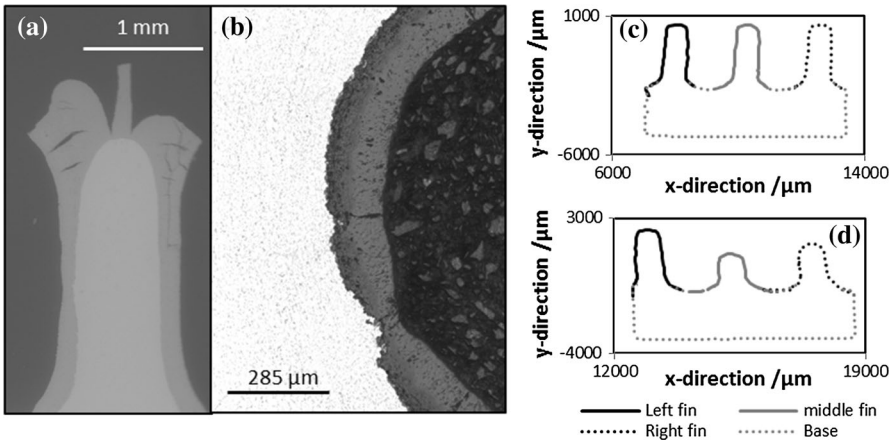

Fig. 2 Variation in oxidation/carburisation is common. **a** The fin tip has started breakaway oxidation, while the fin sides continue to form duplex oxide. **b** Thickness variation in duplex oxidation is common. **c** Measurements of the inner oxide/metal interface for a 3-finned sample after exposure at 600 °C for 12,877 h shows little loss of metal from its fins (**d**) however, the effect of the same exposure after 19,924 h results in more significant fin metal loss (extent varying from fin-to-fin)

When applying the dimensional metrology technique, it is important to clearly define the different layers of interest. The outer magnetite (Fe_3O_4) typically appears to have a slightly lighter grey-scale in optical microscopy and a different pore structure to the inner spinel ($(Fe,Cr)_3O_4$). In duplex oxidation, the two layers have similar thicknesses. However, for the development of complex oxide structures (indicating the onset of breakaway oxidation), this one-to-one thickness ratio breaks down. This is due, in part, to defining the inner oxide as containing any non-standard oxidation products/scales such that any breakaway products are accounted for in this measurement.

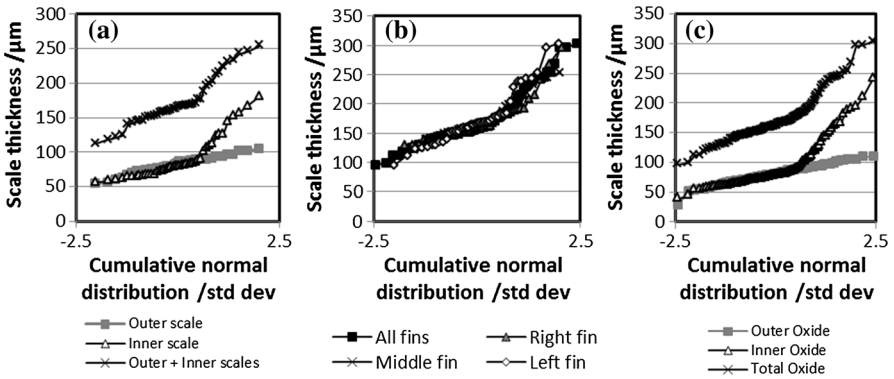

Fig. 3 Dimensional metrology data from a 3-finned sample exposed for 12,877 h at 640 °C. **a** The variation in different oxide thicknesses around one fin. **b** A comparison of total oxide thickness for the three different fins, as well as the combined, 3-fin, dataset. **c** The variation in different oxide thicknesses for all 3 fins of the sample

Figure 3 gives examples of this dimensional metrology data for a sample exposed for 12,877 h at 640 °C. Looking at one single fin (Fig. 3a), the outer oxide (magnetite) shows a continuous normal distribution of scale thickness measurements (indicated by a straight line when plotted against cumulative normal distribution) and a median magnetite thickness value of 80 μm. By contrast, the inner (spinel, when measuring duplex oxidation) layer shows two distinct regions. The first overlays the magnetite distribution and corresponds to measurements taken from locations where the fin was experiencing duplex oxidation. (Note that this also includes the median value.) The second region shows much thicker oxide layers (up to 180 μm) and indicated that breakaway oxidation was occurring. One of the strengths of using this dimensional metrology method is that it is possible to continue to monitor the growth of the duplex oxide despite regions of the sample (typically around the fin tip) having entered breakaway. The total oxide thickness is the sum of the inner and outer oxide layers (from the measurements taken prior to reordering to determine the cumulative probability).

Comparison between different fins of a sample (Fig. 3b) indicates similar median and variance values. As such, data from all fins on a sample can be considered to be one, much larger, dataset. Figure 3c shows these larger and more statistically significant distributions in scale thicknesses for inner, outer and total oxides for the sample. These datasets can be used for comparison between samples exposed to different autoclave conditions.

For example (Fig. 4), the effect of increasing exposure time can be studied. As exposure time increases, the thicknesses of both the inner and outer duplex oxides increase, as does the fraction of the sample undergoing breakaway oxidation. The apparent exceptions to the trend of increasing breakaway with exposure time are the samples at 16,905 and 19,924 h. In this instance, the sample exposed for 19,924 h has started to show significant metal loss around the fin tips, which makes collecting breakaway oxide measurements more difficult, resulting in less measurements of breakaway oxide than are found for the 16,905 h sample.

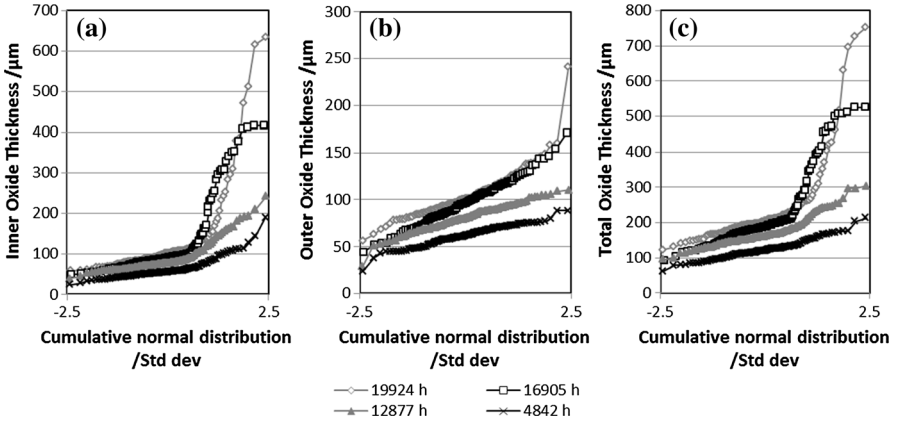

Fig. 4 Dimensional metrology data from four different 3-finned samples exposed at 600 °C for various times, showing the spreads in **a** inner oxide thickness; **b** outer oxide thickness; and **c** total oxide thickness

Effect of Exposure Conditions

Data from autoclaves operated at 600, 620 and 640 °C indicate that the measured total oxide thickness increases with temperature (Fig. 5). By plotting the square of the median total oxide thickness against time, it is apparent that the growth kinetics are approximately parabolic, assuming an offset from zero. Such an offset may be partially explained by the anticipated formation of more rapidly growing transient oxides at very short exposure times.

There is a significant difference between the median total oxide thicknesses at the three temperatures after the same exposure time. After ~1500 h, total oxide scale's median value is ~70 μm at 600 °C, ~97 μm at 620 °C, and ~130 μm at 640 °C. The AGR operational temperatures are lower than the simulated AGR conditions, and so it can be surmised that significantly lower oxide thicknesses will develop in plant; furthermore, as the spinel and magnetite grow ~1:1, and as the only the spinel layer is inward growing, the spinel thickness is equivalent to metal consumed, meaning that the metal loss will only be approximately half the total oxide thickness (for duplex oxidation).

In Fig. 6, the impact of trace 'moisture' on duplex oxidation is considered. There is no significant difference between the two 'moisture levels', which may be a result of the similar oxygen partial pressures in both gas compositions, compared to the variation from changing temperature. However, the finned tube samples show slower oxide growth (smaller oxide thicknesses) than the plain tube samples. It is believed that this relates to the slightly different compositions (see Table 1) of these two batches of alloys.

Discussion Relating to Carbon Injection

The AMEC/EDF sample archive is extensive. Figure 7 plots data from all samples measured to date using the dimensional metrology technique. The plot shows the

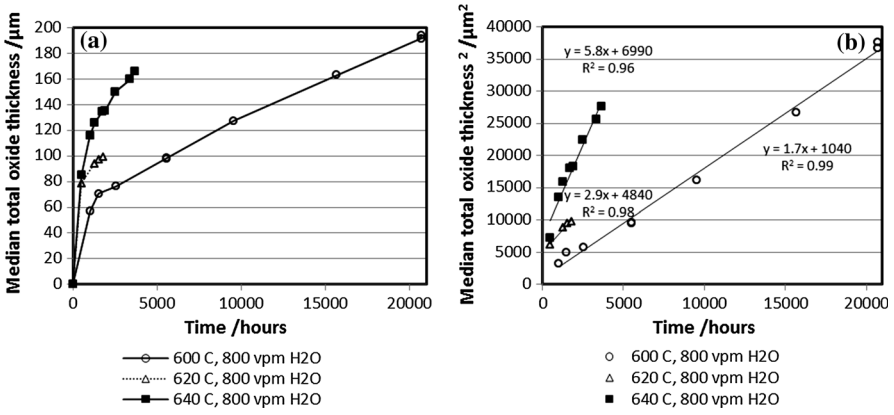

Fig. 5 Effect of varying the autoclave temperature on duplex oxide scale growth. **a** Median total scale thicknesses from dimensional metrology data. **b** Squared median total oxide thickness against time

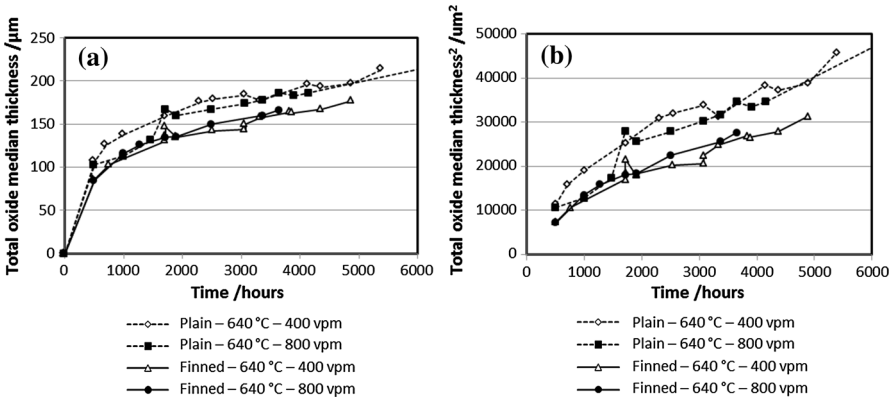

Fig. 6 Effect of varying autoclave 'moisture' content and tube type on duplex oxide scale growth. **a** Median total scale thicknesses from dimensional metrology data. **b** Squared median total oxide thickness

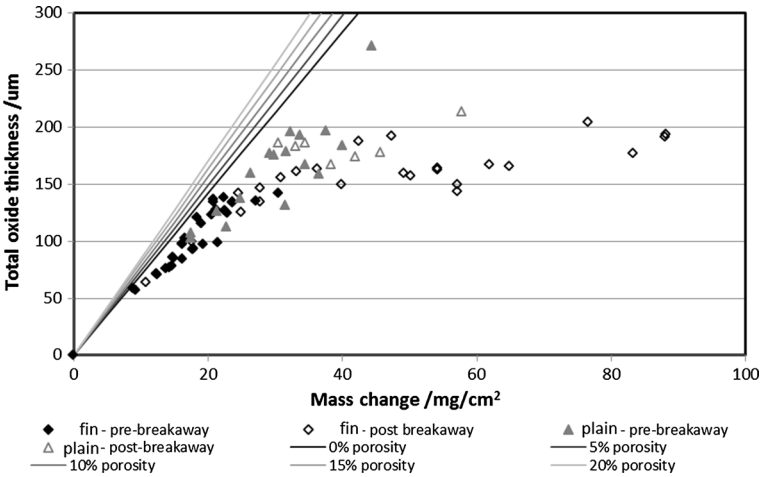

Fig. 7 (*Symbols*) Comparison of recorded sample weight changes and measured median total oxide thicknesses for various autoclave samples. (*Lines*) The theoretical relationship between mass change and total oxide thickness assuming the entire scale to be magnetite with a density of 5.17 g/cm^3 (*black*: maximum density; *light grey*: porosity at 20%)

relationship between the recorded sample weight change and the measured median scale thickness. These samples follow a clear trend, until a weight change of $\sim$25 mg cm^{-2}, when breakaway oxidation initiates on the finned samples. Also plotted in Fig. 7 is the relationship between mass change and total oxide thickness (here assuming that both the magnetite and spinel have the same density, 5.17 g/cm^3). Different lines are plotted using Eq. 3 assuming different oxide scale porosities (0–20%) from an initial, fully dense magnetite oxide.

$$\Delta w = \rho t \left(\frac{100 - x}{100} \right) \quad (3)$$

where Δw is the weight change (in mg/cm^2); ρ is the density of the scale (in mg/cm^3); t is the oxide thickness (in cm); and x is the fraction of porosity (in %).

As increasing porosity is assumed in the oxide, the total oxide thickness for a given weight change increases. By contrast, all recorded median total oxide scale thicknesses fall below the fully dense (0% porosity) line, i.e. all measured samples have thinner oxides than expected from their weight change. It is believed that this additional weight gain has come from the carbon taken up by the base alloy. This extensive carburisation can be observed in optical micrographs, both with and without etching and is coupled to the oxidation reactions that form the duplex oxide layers.

Conclusions

The dimensional metrology technique has been successfully applied to study duplex oxide thickness development in 9Cr-1Mo ferritic steel samples exposed to environments representative of UK AGR operation. In particular, it gives useful information on the spread of oxide thicknesses, the development of oxide layers with time and the initiation of breakaway oxidation mechanisms.

Data from this analysis (such as the median oxide scale thicknesses) can be used to investigate the underlying oxidation growth kinetics. Current work indicates parabolic relationships, which are depended upon temperature and sample type, but have only limited dependence on trace 'moisture' in the test gas environment.

Finally, by comparing the measured relationship between sample mass gain and oxide growth and making comparison to theoretical oxide thicknesses, it is possible to infer the extent of base alloy carburisation. As carburisation of the base alloy has been hypothesised to be responsible for the initiation of breakaway oxidation, this relationship should be pursued further, taking into account geometrical factors.

Acknowledgements The authors gratefully acknowledge funding for this work received from EDF Energy Generation.

References

1. P. Banks, The Oxidation and Carburisation of 9%Cr-1%Mo Steels at Temperatures between 480 and 650 °C in CO/CO_2, Ph.D. Thesis (University of Manchester, 1981).
2. J. Glasgow, K. England and M. Wood, *Gas-Cooled Reactors Today*, vol. 4 (BNES, London, 1983), p. 69.

3. D. R. Holmes, D. Mortimer and J. E. Newell, *Corrosion of Steels in CO_2* (BNES, London, 1974), p. 151.
4. J. W. Taylor, *Gas-Cooled Reactors Today*, vol. 4 (BNES, London, 1983), p. 183.
5. G. B. Gibbs and L. A. Popple, *Nuclear Energy* **21**, 51 (1982).
6. P. L. Harrison, R. B. Dooley, S. K. Lister, D. B. Meadowcroft, P. J. Nolan, R. E. Pendlebury, P. L. Surman and M. R. Wooton, *Corrosion of Steels in CO_2* (BNES, London, 1974), p. 220.
7. N. Birks, G. H. Meier and F. S. Pettit, *Introduction to the High-Temperature Oxidation of Metals* (Cambridge University Press, Cambridge, 2006).
8. D. J. Young, *High Temperature Oxidation and Corrosion of Metals* (Elsevier Corrosion Series, Elsevier, Amsterdam, 2008).
9. P. C. Rowlands, D. R. Holmes, A. Whittaker, R. A. Brierley and J. C. P. Garrett, *Gas-Cooled Reactors Today*, vol. 4 (BNES, London, 1983), p. 173.
10. P. A. Harrigan, The Oxidation and Carburisation of Fe9Cr1Mo Steels in High Pressure, High Temperature Carbon Dioxide, M.Sc. thesis (University of Manchester, 1986).
11. T. Gheno, Oxidation and Carburisation of Model Chromia-Forming Alloys in Carbon Dioxide, Ph.D. Thesis (The University of New South Wales, 2012).
12. F. Rouillard, G. Moine, L. Martinelli and J. C. Ruiz, *Oxidation of Metals* **77**, 57 (2012).
13. A. M. Pritchard and A. E. Truswell, *Corrosion of Steels in CO_2* (BNES, London, 1974), p. 234.
14. R. A. Brierley, *Corrosion of Steels in CO_2* (BNES, London, 1974), p. 165.
15. G. A. Camona, M. Imbergamo and C. Ronchetti, *Corrosion of Steels in CO_2* (BNES, London, 1974), p. 45.
16. B. Dewanckel, D. Leclercq and J. Dimier, *Corrosion of Steels in CO_2* (BNES, London, 1974), p. 42.
17. P. A. German and A. C. Littlejohn, *Corrosion of Steels in CO_2* (BNES, London, 1974), p. 1.
18. P. A. German, A. Hill and M. Taylor, *Gas-Cooled Reactors Today*, vol. 4 (BNES, London, 1983), p. 169.
19. P. C. Rowlands, J. C. P. Garrett, F. G. Hicks, S. K. Lister, B. Lloyd and J. A. Twelves, *Corrosion of Steels in CO_2* (BNES, London, 1974), p. 193.
20. N. O. Grandison and R. I. Facer, *Corrosion of Steels in CO_2* (BNES, London, 1974), p. 208.
21. Various, *Corrosion of Steels in CO_2* (BNES, London, 1974), p. 279.
22. M. G. C. Cox, B. McEnaney and V. D. Scott, *Corrosion of Steels in CO_2* (BNES, London, 1974), p. 247.
23. H. Al-Badairy, G. J. Tatlock and M. J. Bennett, *Materials at High Temperature* **17**, 101 (2000).
24. EC JOULE Project, *Erosion/Corrosion of Advanced Materials for Coal-fired Combined Cycle Power Generation*, Report: JOUF-0022, Final & Summary Reports, 1993.
25. N. J. Simms, J. E. Oakey, D. J. Stephenson, P. J. Smith and J. R. Nicholls, *Wear* **186**, 247 (1995).
26. N. J. Simms, J. E. Oakey and J. R. Nicholls, *Materials at High Temperatures* **17**, 2000 (355).
27. N. J. Simms, P. J. Smith, A. Encinas-Oropesa, S. Ryder, J.R. Nicholls and J. E. Oakey, in *Lifetime Modelling of High Temperature Corrosion Processes*, *Proceedings of European Federation of Corrosion Workshop*, Vol. 34 (European Federation of Corrosion Publication, 2001), p. 246.
28. A. U. Syed, N. J. Simms and J. E. Oakey, *Fuel* **101**, 62 (2012).
29. J. Sumner, A. Encinas-Oropesa, N. J. Simms and J. R. Nicholls, *Oxidation of Metals* **80**, 553 (2013).
30. J. Sumner, A. Potter, N. J. Simms and J. E. Oakey, *Materials at High Temperatures* **32**, 177 (2015).
31. D. J. Hand, *Statistics: A Very Short Introduction* (Oxford University Press, UK, 2008).
32. M. Kowaka, *Introduction to Life Prediction of Industrial Plant Materials* (Allerton Press, New York, 1994).
33. J. Sumner, N. J. Simms, A. Shin and J. Pearson, *Proceeding SMiRT-23* (Manchester, UK, 2015).
34. F. Rouillard and L. Martinelli, *Oxidation of Metals* **77**, 77 (2012).